ACS OMEGA

Open Access

http://pubs.acs.org/journal/acsodf

Article

Desorption Characteristics of CH_4−C_2H_6 Mixed Gas in Heavy Hydrocarbon-Rich Coal Seams

Yuehui Liang,* Biming Shi, Jiwei Yue,* Chengcheng Zhang, Xiaojing Shen, Tao Hu, and Qijun Han

Cite This: *ACS Omega* 2024, 9, 16176−16186

Read Online

ACCESS | Metrics & More | Article Recommendations

ABSTRACT: The gas desorption characteristics of coal are closely related to the gas content of the coal seam. The gas in heavy hydrocarbon-rich coal seams contains CH_4 and C_2H_6 heavy hydrocarbons. However, most current research on the gas desorption characteristics of coal seams focuses on CH_4 analysis, ignoring the influence of the C_2H_6 heavy hydrocarbon gas. To accurately determine the gas content of a heavy hydrocarbon-rich coal seam, methods based on CH_4 analysis are inadequate and the desorption characteristics of CH_4−C_2H_6 mixed gas must be clarified. This work experimentally and theoretically studies the desorption characteristics of single-component gas and CH_4−C_2H_6 mixed gas from coal samples. The results show that increasing the adsorption-equilibrium pressure was found to increase the desorption quantity and desorption speed of single-component gas and increase the desorption quantity, desorption ratio, and diffusion coefficient of mixed gas. Under the same adsorption-equilibrium pressure, the desorption quantity and rate of single-component CH_4 gas exceeded those of C_2H_6. The quantity and speed of mixed gas desorption increased with rising CH_4 concentration and decreased with rising C_2H_6 concentration. The change in the mixed gas concentration during desorption reflects the distribution characteristics of light hydrocarbon components on the outer surface and heavy hydrocarbon components on the inner surface of coal. From the desorption characteristics of mixed gas, desorption models of mixed gas were obtained at different concentrations, laying a theoretical foundation for accurate determinations of gas contents in heavy hydrocarbon-rich coal seams.

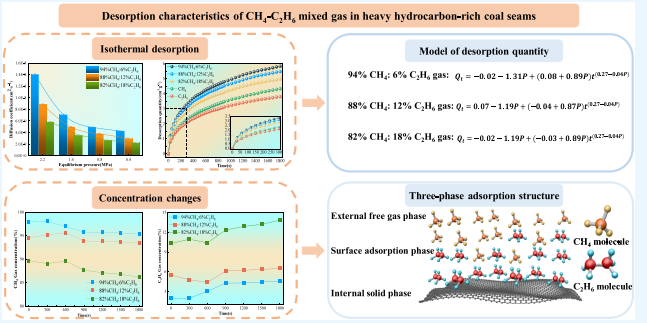

1. INTRODUCTION

Although coal is the stabilizer and ballast of energy security, coal and gas protrusions in the mining process seriously restrict the safe production of coal mines and endanger the occupational safety and health of workers.[1−3] In the prevention and control of coal and gas herniation, the gas content of the coal seam is a critical indicator of gas outflow from mines. The gas content enables predictions of areas at risk of coal and gas herniation, along with effectiveness evaluations of antidisruptive measures.[4−6] Moreover, the safety requirements are tightening with the increasing depth of coal mining, and the reliability and accuracy of the coal bed methane content measurement results are paramount.

The gas components of coal seams are roughly divisible into hydrocarbons and nonhydrocarbons.[7] The hydrocarbons (mainly CH_4 and a certain amount of heavy hydrocarbon gas) dominate, while nonhydrocarbon gases (such as CO_2 and N_2) exist in small amounts.[8−10] According to recent research based on industrial tests for measuring the gas contents of coal seams,[11] the proportion of heavy hydrocarbon gas reaches 5−25% in some mining areas. The characteristics and causes of heavy hydrocarbon gas have been extensively researched. For example, Lan et al. reported a heavy hydrocarbon gas content of 2.9−36.98% in part of the exploration area of the Enhong Slope of Yunnan.[12] Gentzis et al. measured a C_2H_6 concentration of 5.2−7.9% in the coal seam of Alberta, Canada.[13] They considered that heavy hydrocarbon gas results from the penetration of gas from oil (gas) reservoirs into the coal seam. Formolo et al. reported a heavy hydrocarbon gas content of 5−15% in the coal seam in the southwestern and northwestern part of the San Juan Basin of the United States, possibly arising from contact metamorphism of igneous rock intrusion.[14] An on-site gas geological exploration by Wang et al. and Fu et al. found that heavy hydrocarbon gas anomalies in the coal seam in China amounted to 5.16%.[15,16] Numerous data analyses have identified a positive correlation between the heavy hydrocarbon gas content and buried depth, suggesting that heavy hydrocarbon gas is the product of plant transformation into coal.

Received: December 19, 2023
Revised: March 7, 2024
Accepted: March 13, 2024
Published: March 25, 2024

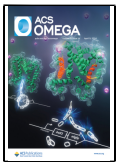

Most scholars simulate the occurrence of coal seam gas based on single-component gases such as CH_4, CO_2, and N_2, along with mixtures of these gases. Wang et al. and Ji et al. carried out isothermal adsorption measurements of high-pressure CH_4.[17,18] They found that the temperature and equilibrium pressure affect the limiting adsorption quantity. Wang et al. believed that CO_2 adsorption increases the intensity of shear vibrations, causing irreversible damage to defective parts of the coal body.[19] They proposed a molecular mechanism for the deformation of the CO_2-adsorbed coal. Zhang et al. analyzed the multiple fractal characteristics of the pore structures of coals with different degrees of coalification during N_2 adsorption.[20] The pores became increasingly complex with an increasing coalification degree. Yu et al. conducted an adsorption−desorption experiment of CH_4−CO_2 mixed gas; they found the concentration of CH_4 in the desorption gas was always more significant than that of CO_2, which was considered to be closely related to the microscopic composition and coal rank.[21] Li et al. simulated the adsorption of CH_4−N_2 mixed gas on coal through triaxial stress tests, found that the coal body expanded and deformed, and the strength of the coal body decreased.[22] Combining the results of CO_2−N_2 adsorption experiments with molecular dynamics software, Xu et al. constructed microporous and mesoporous models of the loading and migration processes, and they proposed the dual adsorption mechanism of N_2−CO_2.[23] Long et al. studied the adsorption process of mixed gas on different coal samples through a competitive mixed gas adsorption experiment.[24] According to the Yoon−Nelson model of single-component gas, they found that the mass transfer rate decreases in the order of N_2 > CH_4 > CO_2.[25] Most research on gas desorption from coal is based on the CH_4. For instance, Li et al. investigated the effect of pore structure on the diffusion coefficient of CH_4 in coals of different ranks, and they found that the diffusion coefficient of CH_4 increased first and then decreased with the increase of coal rank.[26] Liu et al. believed that coal pores have bimodal characteristics, proposed a double diffusion model to describe the desorption process of CH_4 from coal.[27] Guatame et al. related the CH_4 concentration to the petrographic characteristics of coal.[28] They found that gas desorption from the coal seam is related to the microcomponent composition of coal. Sun et al. experimentally studied CH_4 desorption under positive pressure conditions (relative to atmospheric pressure).[29] They reported an increasing quantity of gas desorption with an increasing relative desorption pressure.

Heavy hydrocarbon gas has received insufficient attention in coal seam gas research. Few studies have considered the gas desorption law in heavy hydrocarbon-rich coal seams or the desorption characteristics of heavy hydrocarbon CH_4 mixed gas at different concentrations. Isothermal adsorption−desorption experiments of coal typically employ CH_4 and other single-component gases.[30] As the obtained adsorption−desorption characteristics cannot properly reflect the actual energy-storage situation in heavy hydrocarbon-rich coal seams, the accuracy of the gas content determination is compromised. Therefore, obtaining the desorption characteristics of heavy hydrocarbon gas is necessary to determine the gas content in heavy hydrocarbon-rich coal seams and prevent coal and gas outburst work.

The contents of hydrocarbon gas components in coal seam gas decrease in the order of CH_4 > C_2H_6 > C_3H_8 > C_4H_{10}. More than 90% of the heavy hydrocarbon gas is C_2H_6; the remaining straight-chain alkanes are present in small amounts.[31−33] Therefore, the present study selects C_2H_6 as the research subject and constructs an experimental platform for investigating CH_4−C_2H_6 mixed gas desorption. To investigate the desorption characteristics of CH_4−C_2H_6 mixed gas in the coal seam, three mixed gases—94%CH_4:6%C_2H_6, 88%CH_4:12%C_2H_6, and 82%CH_4:18%C_2H_6—were subjected to isothermal desorption experiments. The results lay a theoretical foundation for accurate gas content determinations in heavy hydrocarbon-rich coal seams.

2. EXPERIMENTAL METHODOLOGY

2.1. Coal Sample Preparation. The coal sample was taken from the 13-1 coal seam in the Panji Coal Mine of Huainan Mining Group, located in the eastern section of the synclinorium of Huainan Coalfield and the deep part of the turning end of the Chenqiao−Panji anticline.[34] The fault-structure development in the coalfield is dominated by longitudinal oblique faults. The faults lie parallel to the anticline axis, and the angle between the fault intersection line and coal seam strike is small.[35,36] The complex tectonic stress is relatively concentrated because the minefield is located at the turning−overturning end of the anticline. The content of heavy hydrocarbon gas in the coal seam ranges from 5.58 to 17.07% and is higher in the deep part of the mine (<1000 m) than in the shallow part. In contrast, the CH_4 content is lower in the deep part than in the shallow part.[37] The local strata in the sampling area and mine structure information are listed in Figure 1.

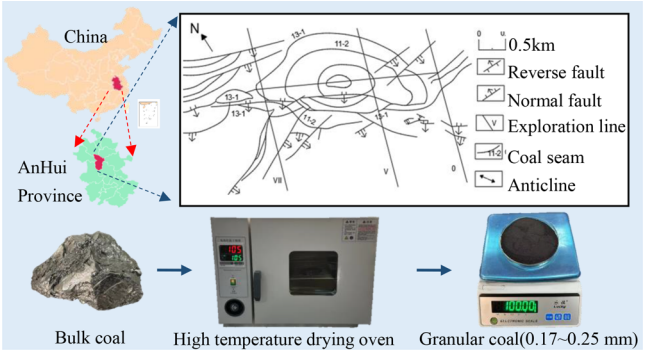

Figure 1. Sampling location and preparation of the coal samples.

Coal sample production steps: (1) After sampling at the working face, the sample tank is immediately sealed and transported to the laboratory. (2) The coal block is crushed in a crusher, and particles of diameter 0.17−0.25 mm are selected through a vibrating screen. (3) The coal sample is placed in a 105 °C drying oven for 12 h. (4) The dried coal sample is placed in a weighing dish, and the coal sample tank is filled with 100g of sample.[38]

After screening and drying the remaining coal samples, the coal samples were analyzed followed the industrial standard "Proximate Analysis of Coal" (GB/T212-2008).[39] The adsorption constants of the coal samples (Table 1) were determined following the "Experimental Method of High-Pressure Isothermal Adsorption to Coal" standard (GB/T19560-2008).

2.2. Experimental System. On a designed adsorption−desorption experimental platform, the authors determined the desorption quantities of single-component CH_4 gas and C_2H_6 gas, along with the desorption characteristics and concentration changes of CH_4−C_2H_6 mixed gas. The experimental platform maintains the experimental gas and coal samples at constant

https://doi.org/10.1021/acsomega.3c10156
ACS Omega 2024, 9, 16176−16186

Table 1. Parameters Elated to the Coal Samples

			gas adsorption constant			
M_{ad} (%)	A_{ad} (%)	V_{daf} (%)	classification of gases	a ($cm^3 \cdot g^{-1}$)	b (MPa^{-1})	R^2
1.92	18.24	24.59	94%CH_4:6%C_2H_6	20.5815	0.5415	0.9984
			88%CH_4:12%C_2H_6	20.4792	0.6262	0.9895
			82%CH_4:18%C_2H_6	20.0810	1.0573	0.9949
			CH_4	19.4310	1.1704	0.9919
			C_2H_6	18.7152	1.4631	0.9926

temperature and performs real-time monitoring of the gas desorption data, detection of desorption gas concentration, and dead-volume calibration (Figure 2).

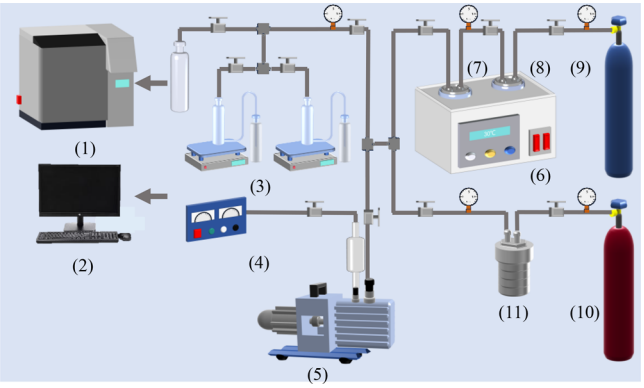

Figure 2. Adsorption−desorption experimental platform for CH_4−C_2H_6 mixed gas: (1) chromatograph, (2) data acquisition system, (3) desorption meter, (4) vacuum gauge, (5) vacuum pump, (6) thermostat water bath, (7) coal sample tank, (8) buffer tank A, (9) gas cylinder A, (10) buffer tank B, and (11) gas cylinder B.

2.3. Experimental Procedure.

1. Adsorption equilibrium: After injecting helium gas into cylinder B for leakage check, the coal sample tank and pipeline were pumped to a vacuum of <30 Pa using a vacuum pump. Ensuring that the water bath had stabilized at 30 °C, the preprepared mixed gas was filled into buffer tank A through cylinder A, and the valve was closed after reaching the target pressure. When the pressure-sensor parameters remained constant for more than 4h, the gas in buffer tank A was assumed to have reached stable state. The valve was then opened to connect the buffer tank A to the coal sample tank. While filling the coal sample tank with gas, the equilibrium pressure changes in the tank were observed and recorded until adsorption equilibrium at the target pressure was reached. Subsequently, the valve was opened and buffer tank A was connected to the coal sample tank for charging the gas. Again, the equilibrium pressure change in the coal sample tank was recorded until the coal sample reached adsorption equilibrium at the target pressure.
2. Atmospheric desorption: The valve was adjusted to desorb the gas from the coal samples in the tank under atmospheric pressure. The released gas was collected by a desorption meter. The cumulative desorption time was 1800s, and the data-saving period was 30s during the first 900 and 60s during the last 900s. To compare and analyze the desorption behaviors of different gas components, the measured desorption quantity was converted to the standard condition as follows:

$$Q_t = \frac{273.15}{0.101325(273.15 + T)M} P_0 \cdot Q_t' \quad (1)$$

where Q_t is the desorption volume under standard conditions (cm^3/g), T is the room temperature (°C), M is the mass of the coal sample (g), P_0 is the room atmospheric pressure (MPa), and Q_t' is the measured volume (cm^3).

3 Chromatographic analysis: The gas components released by desorption of a mixed gas must be analyzed within a certain period. To ensure accurate desorption measurements, the gas was collected in different gas cylinders during different periods. After a predetermined time, the previous valve was quickly closed and the latter valve was opened to admit the desorption gas to the next cylinder.

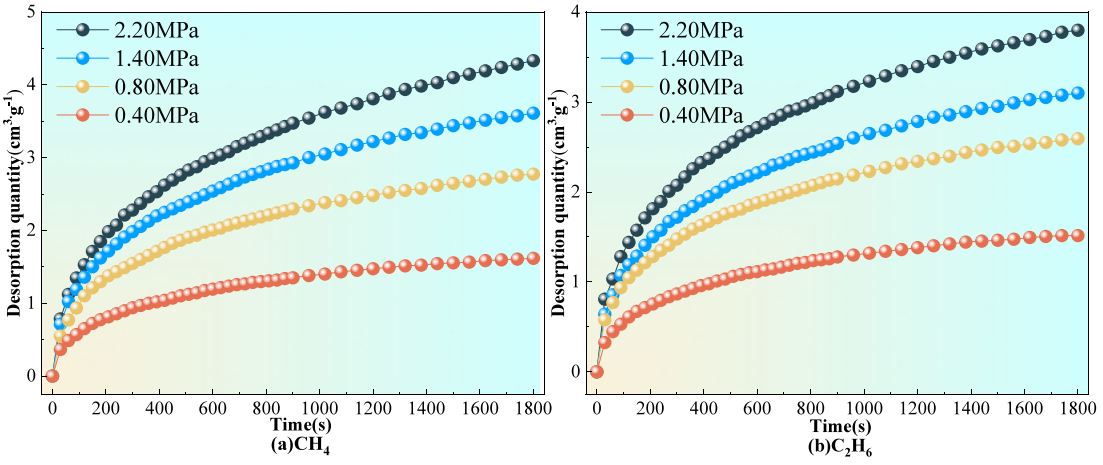

Figure 3. Temporal changes in desorption quantities of single-component gas, derived from the data of desorption experiments.

https://doi.org/10.1021/acsomega.3c10156
ACS Omega 2024, 9, 16176−16186

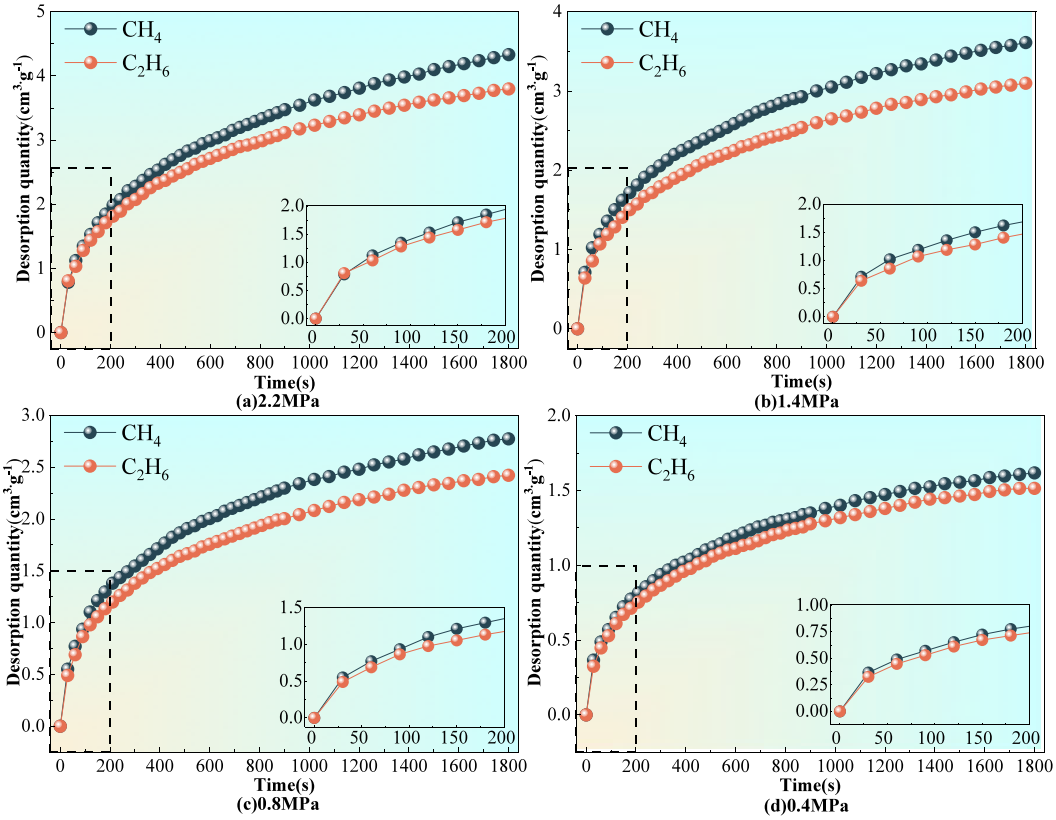

Figure 4. Temporal changes in desorption quantities of CH_4 and C_2H_6 during single-component gas desorption experiments under the same adsorption-equilibrium pressure.

The gas in the corresponding gas cylinder was collected in a gas collection bag and connected to a gas chromatograph for concentration analysis.

3. RESULTS AND DISCUSSION

3.1. Isothermal Desorption Analysis of Single-Component Gas. Isothermal (30 °C) desorption experiments of CH_4 and C_2H_6 were conducted at different adsorption-equilibrium pressures (2.2, 1.4, 0.8, and 0.4 MPa). Figure 3 plots the desorption quantities of the single-component gas as a function of time.

Under different adsorption-equilibrium pressures, the isothermal desorption processes of the single-component gas show similar desorption characteristics. Increasing the adsorption-equilibrium pressure increased both the desorption speed and desorption quantity in the initial stage and amplified the upward trend of the desorption curve. The initial rapid decay in the desorption process slowed after 1200s, and the desorption quantity gradually tended to its limit value. Because the desorption values of CH_4 and C_2H_6 obviously differed over the same period, they were analyzed and compared at the same adsorption-equilibrium pressure. The results are shown in Figure 4.

At the same adsorption-equilibrium pressure, the quantity and speed of CH_4 desorption exceeded those of C_2H_6 desorption. At adsorption-equilibrium pressures of 2.2, 1.4, 0.8, and 0.4 MPa, the cumulative desorption volume differences between CH_4 and C_2H_6 were 0.53376, 0.51264, 0.35252, and 0.10322 cm^3/g, respectively. The differences gradually decrease with decreasing adsorption-equilibrium pressure, and the results of CH_4 and C_2H_6 are close when the adsorption-equilibrium pressure reaches 0.4 MPa.

Coal is an adsorbent with an apparent molecular-sieve effect. CH_4 molecules are small, simply structured, and lightweight, whereas C_2H_6 molecules are large, complex, and weighty. As the migration and flow resistances of CH_4 are small, CH_4 molecules desorb in a higher quantity at higher speed than C_2H_6 molecules. As the adsorption-equilibrium pressure decreases, gas exchange between the adsorbed and free phases is weakened, and the transport process of the CH_4 and C_2H_6 molecules slows. Accordingly, the desorption quantities and speeds of CH_4 and C_2H_6 converge at low adsorption-equilibrium pressures.

3.2. Isothermal Desorption Analysis of CH_4–C_2H_6 Mixed Gas. *3.2.1. Change Rules of the CH_4–C_2H_6 Mixed Gas Desorption Quantity.* Under the conditions of the actual situation,[37] three groups of mixed gases (94%CH_4:6%C_2H_6, 88%CH_4:12%C_2H_6, and 82%CH_4:18%C_2H_6) were prepared and subjected to desorption experiments at different adsorption-equilibrium pressures (2.2, 1.4, 0.8, and 0.4 MPa). The temporal changes in desorption quantities of the mixed gases are plotted in Figure 5.

Under the same adsorption-equilibrium pressure conditions, the initial desorption speed and cumulative desorption of the CH_4–C_2H_6 mixed gas gradually increased with an increasing CH_4 concentration. In contrast, the desorption quantity and later desorption speed of the CH_4–C_2H_6 mixed gas decreased with an increasing C_2H_6 concentration.

Next, the multicomponent desorption characteristics were compared with those of the single-component desorption characteristics. Under the same adsorption-equilibrium pressure conditions, the desorption quantity and speed of single-

https://doi.org/10.1021/acsomega.3c10156
ACS Omega 2024, 9, 16176−16186

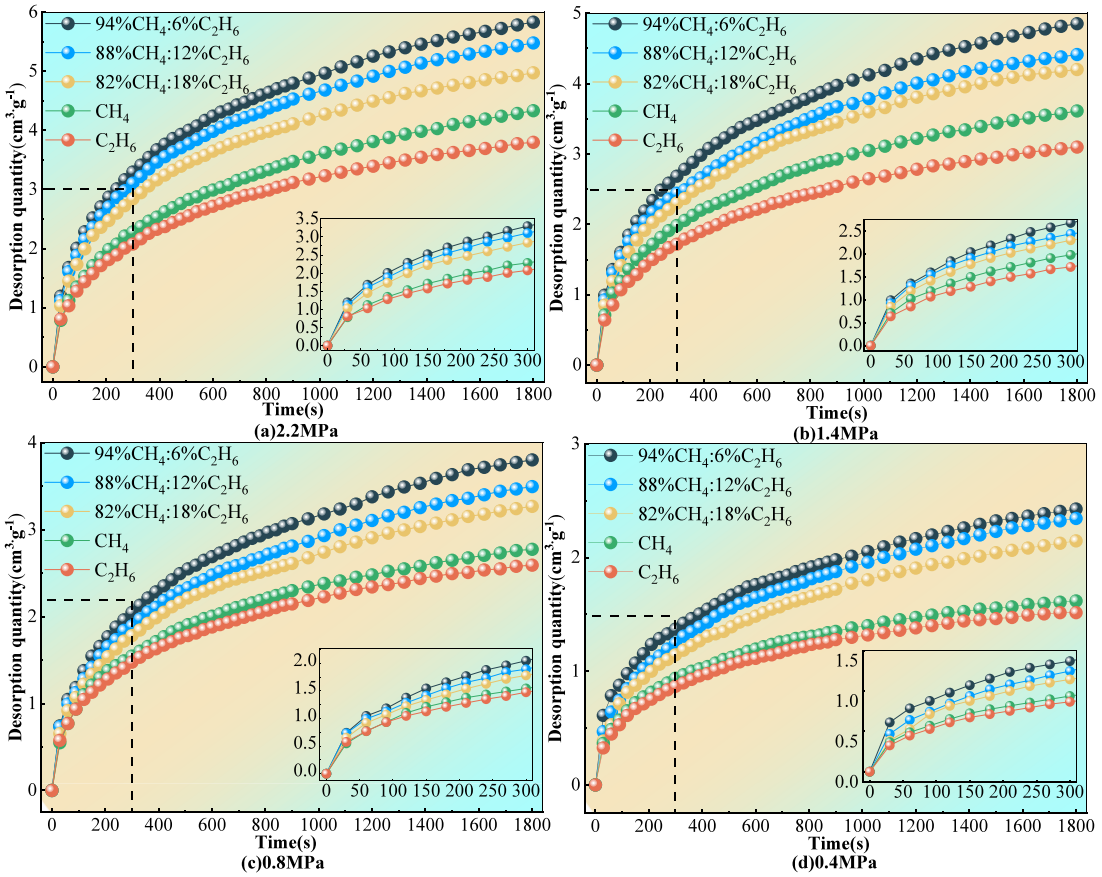

Figure 5. Temporal changes in desorption quantities during the $CH_4-C_2H_6$ mixed gas experiment under the same adsorption-equilibrium pressure.

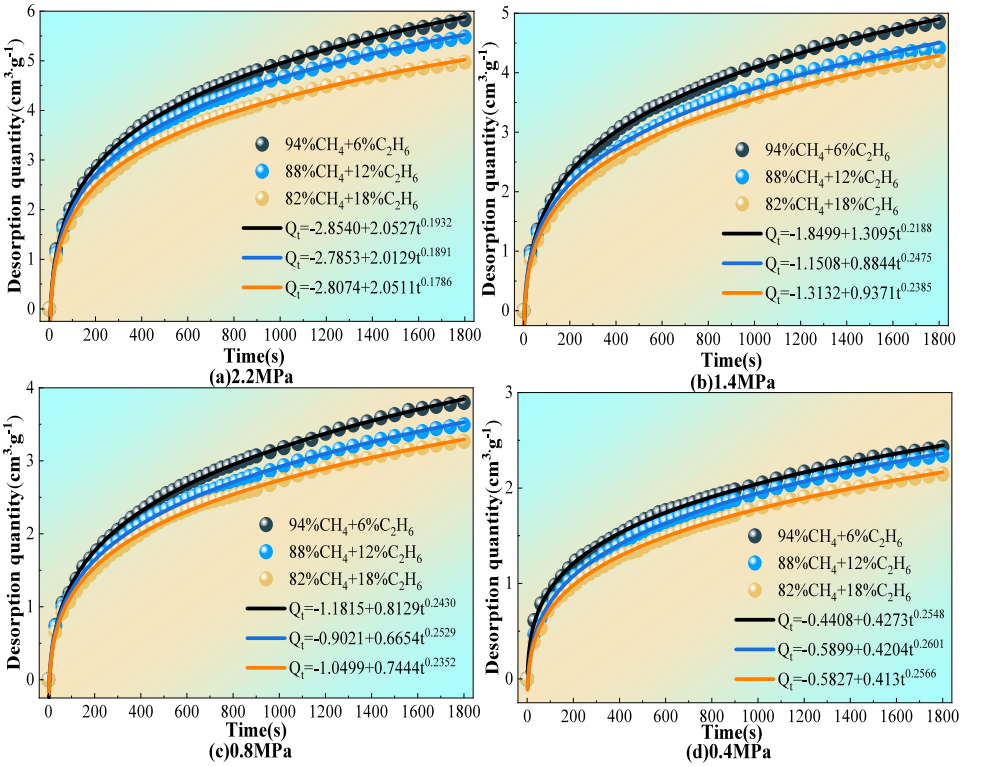

Figure 6. Fitting curve of desorption quantity of $CH_4-C_2H_6$ mixed gas.

https://doi.org/10.1021/acsomega.3c10156
ACS Omega 2024, 9, 16176−16186

component gas in the 1800s before desorption were smaller than those of the CH_4−C_2H_6 mixed gases at all three concentrations. Although the proportion of CH_4 is lower in the mixed gas than in the single-component gas, the pore structures in the heavy hydrocarbon-rich coal body can favor the adsorption of heavy hydrocarbon gases. Hence, heavy hydrocarbon components improve the adsorption effect of the coal body on mixed gas and promote CH_4 desorption. This phenomenon explains the higher desorption results of the mixed gas than of the single-component gas.

3.2.2. Model of CH_4−C_2H_6 Mixed Gas Desorption Quantity. Analyzing the variation rule of the desorbed quantity of mixed gas, one observes that the desorption quantity Q_t increases rapidly with time t before tending to a stable value. Therefore, the desorption quantity Q_t of the CH_4−C_2H_6 mixed gas was fitted to a function of t (eq 2). The fitting curve is shown in Figure 6.

$$Q_t = A + Bt^C \tag{2}$$

Combined with the fitting analysis, the relational expression between the desorption quantity and time of CH_4−C_2H_6 mixed gas with different concentrations under the same adsorption-equilibrium pressure was obtained, and the degree of fit R^2 exceeded 0.998. The constants A, B, and C to be determined are listed in Table 2.

Table 2. Parameters of the Q_t−t Fitting Formula for CH_4−C_2H_6 Mixed Gas

gas category	P (MPa)	A	B	C	R^2
94%CH_4:6%C_2H_6	2.2	−2.8540	2.0527	0.1932	0.9993
	1.4	−1.8499	1.3095	0.2188	0.9992
	0.8	−1.1815	0.8129	0.2430	0.9990
	0.4	−0.4408	0.4273	0.2548	0.9991
88%CH_4:12%C_2H_6	2.2	−2.7853	2.0129	0.1891	0.9993
	1.4	−1.1508	0.8844	0.2475	0.9981
	0.8	−0.9021	0.6654	0.2529	0.9991
	0.4	−0.5899	0.4204	0.2601	0.9991
82%CH_4:18%C_2H_6	2.2	−2.8074	2.0511	0.1786	0.9992
	1.4	−1.3132	0.9371	0.2385	0.9984
	0.8	−1.0499	0.7444	0.2352	0.9989
	0.4	−0.5827	0.413	0.2566	0.9992

In CH_4−C_2H_6 mixed gas with the same concentration ratio, the desorption quantity Q_t of the mixed gas gradually increases with increasing adsorption-equilibrium pressure P. The fitting analysis found a linear relationship between P and the parameters A, B, and C (Table 3).

Substituting the linear relationships in Table 3 into eq 2, the desorption quantity Q_t can be determined at any given desorption time t and adsorption-equilibrium pressure P. The desorption models of the mixed gases with different concentration ratios are given as follows:

(1) Desorption quantity of mixed 94%CH_4:6%C_2H_6 gas:

$$Q_t = -0.02 - 1.31P + (0.08 + 0.89P)t^{(0.27-0.04P)} \tag{3}$$

(2) Desorption quantity of mixed 88%CH_4:12%C_2H_6 gas:

$$Q_t = 0.07 - 1.19P + (-0.04 + 0.87P)t^{(0.27-0.04P)} \tag{4}$$

Table 3. Linear Relationship between Adsorption-Equilibrium Pressure P of the CH_4−C_2H_6 Mixed Gas and the Fitting Parameters A, B, and C

gas category	parameter relationship expression
94%CH_4:6%C_2H_6	A=−0.02 − 1.31P
	B = 0.08 + 0.89P
	C = 0.27 − 0.04P
88%CH_4:12%C_2H_6	A = 0.07 − 1.19P
	B = −0.04 + 0.87P
	C = 0.27 − 0.04P
82%CH_4:18%C_2H_6	A = −0.02 − 1.19P
	B = −0.03 + 0.89P
	C = 0.27 − 0.04P

(3) Desorption quantity of mixed 82%CH_4:18%C_2H_6 gas:

$$Q_t = -0.02 - 1.19P + (-0.03 + 0.89P)t^{(0.27-0.04P)} \tag{5}$$

3.2.3. Change Rules of the CH_4−C_2H_6 Mixed Gas Desorption Ratio. The adsorption-equilibrium pressure evidently influences the desorption process of the CH_4−C_2H_6 mixed gas. Therefore, the desorption ratio changes of the mixed gases were analyzed under different adsorption-equilibrium pressures. The results are listed in Figure 7.

The desorption ratio defines the ratio of the cumulative desorption quantity Q_t to the limit desorption quantity Q_∞. At any given time, Q_∞ denotes the gas desorption quantity at $t \to \infty$, which is the quantity of gas released indefinitely from the coal sample under the adsorption-equilibrium pressure P. During the desorption process at atmospheric pressure (P_0 = 0.1 MPa), Q_∞ is the gas adsorption quantity of the coal sample under the adsorption-equilibrium pressure P_1 and is calculated as

$$Q_\infty = \left(\frac{abP}{1+bP} - \frac{abP_0}{1+bP_0}\right)\cdot\frac{100 - A_{ad} - M_{ad}}{100} \tag{6}$$

where A_{ad} and M_{ad} are the ash and moisture contents of the coal samples, respectively (both in %), and a and b are the adsorption constants of the coal samples under different gas conditions.

Increasing the adsorption-equilibrium pressure gradually increased the desorption ratio and early stage magnitude of the change in the desorption ratio of the CH_4−C_2H_6 mixed gas and also lengthened the equilibrium time. In contrast, decreasing the adsorption-equilibrium pressure caused an earlier slowdown of the desorption ratio curve. Meanwhile, a horizontal asymptote analysis shows that increasing the adsorption-equilibrium pressure increases the limit desorption quantity of the CH_4−C_2H_6 mixed gas.

Heavy hydrocarbon-rich coal easily absorbs and stores heavy hydrocarbon gas. When the adsorption equilibrium is broken, the mixed gas rapidly detaches from the coal body surface and exits through the fissures. During the first 1800s of the desorption process, decreasing the adsorption-equilibrium pressure reduced the adsorption force between the coal body surface and heavy hydrocarbon gas, thereby decreasing the degree of heat exchange between the adsorbed and free-state gas molecules. Accordingly, the desorption ratio curve slowed at an earlier time.

3.2.4. Change Rules of the CH_4−C_2H_6 Mixed Gas Diffusion Coefficient. According to the desorption quantity and desorption ratio change rules of the mixed gas, the desorption process of the CH_4−C_2H_6 mixed gas largely depends on the

https://doi.org/10.1021/acsomega.3c10156
ACS Omega 2024, 9, 16176−16186

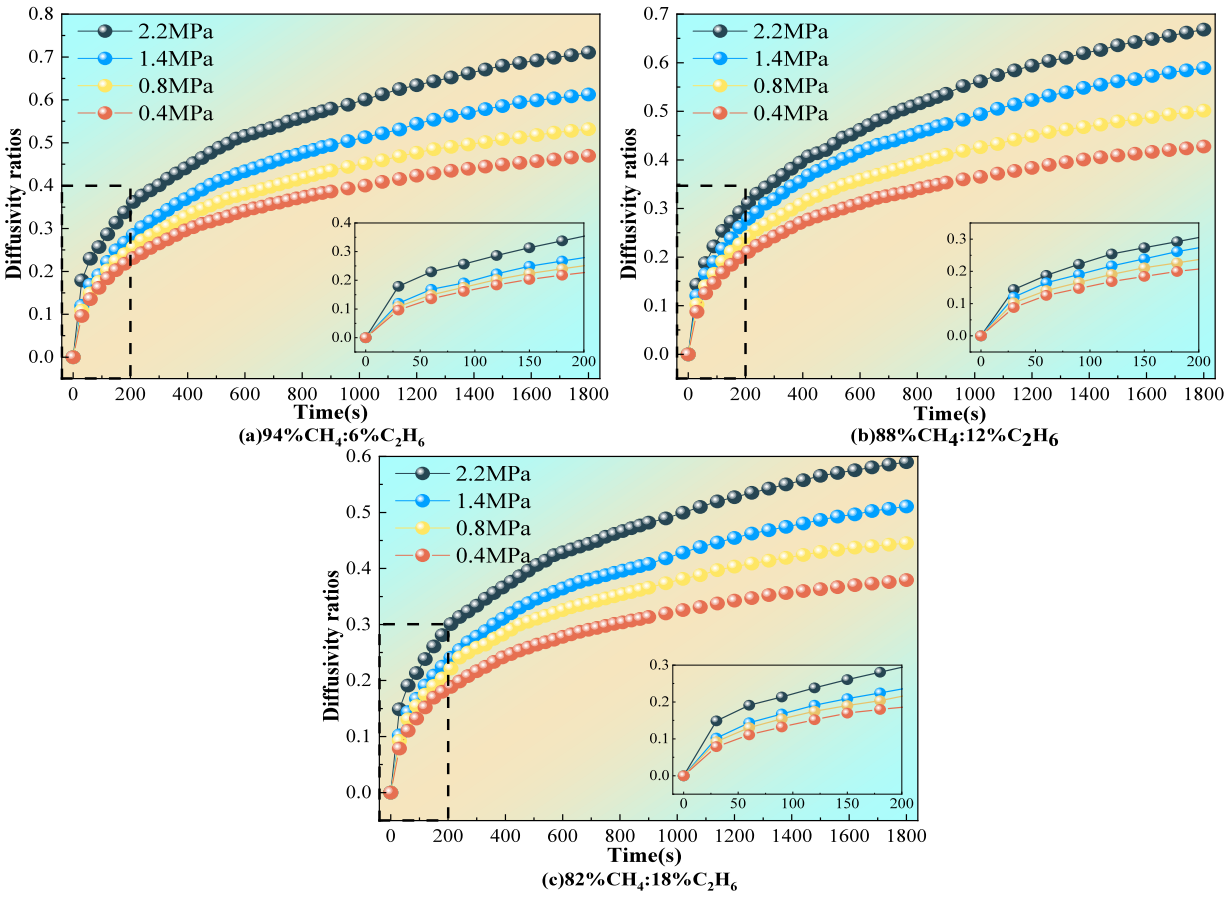

Figure 7. Temporal changes in the desorption ratio during the desorption experiment of CH_4−C_2H_6 mixed gas at the same concentration.

concentration of the heavy hydrocarbon gas. Therefore, the average diffusion coefficient of the mixed gas was analyzed. Based on Fick's second diffusion law, the cumulative desorption quantity Q_t and the limit desorption quantity Q_∞ calculated above are substituted into the classical diffusivity ratios formula for calculations.[40]

$$\frac{Q_t}{Q_\infty} = 1 - \frac{6}{\pi^2}\sum_{n=1}^{\infty}\frac{1}{n^2}e^{-n^2Bt} \tag{7}$$

where t is the desorption time (s), $B = \pi^2 D/R^2$, D is the diffusion coefficient (cm^2/s), and R is the radius of the coal particles (cm). Setting $n = 1$ in eq 7, the diffusion coefficient D becomes a constant. Taking the logarithms of both sides of eq 7 with $n = 1$, we get

$$\ln\left(1 - \frac{Q_t}{Q_\infty}\right) = \ln\left(\frac{6}{\pi^2}\right) - \frac{\pi^2 Dt}{R^2} \tag{8}$$

The average diffusion coefficients of the coal samples with different gas concentrations and adsorption-equilibrium pressures during the first 1800s of desorption were calculated from the linear slopes of $\ln(1-Q_t/Q_\infty)$ versus t plots. The results are listed in Figure 8.

Changing the C_2H_6 concentration in the mixed gas will more likely influence the desorption law of the mixed gas than changing the CH_4 concentration, especially under an adsorption-equilibrium pressure of 2.2 MPa. The diffusion coefficient of the CH_4−C_2H_6 mixed gas in the coal samples

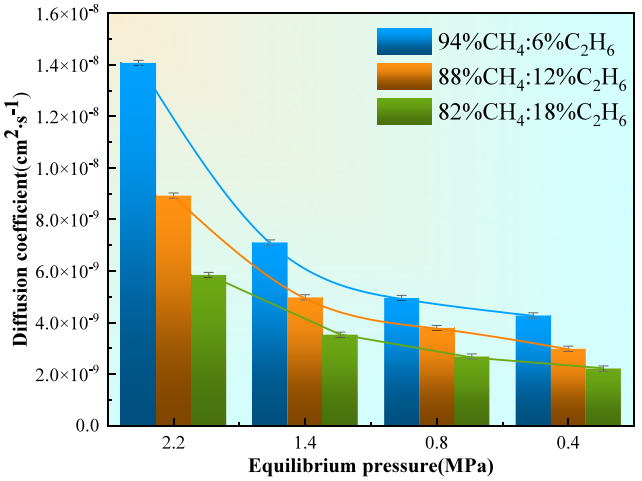

Figure 8. Changes of diffusion coefficient with adsorption-equilibrium pressure during desorption experiments of CH_4−C_2H_6 mixed gas with different concentrations.

gradually decreased with increasing C_2H_6 concentration and decayed with decreasing adsorption-equilibrium pressure.

As the primary pores in the structure of heavy hydrocarbon-rich coal facilitate the storage of heavy hydrocarbon molecules, they can retard the movement of C_2H_6 molecules. Increasing the CH_4 concentration in the mixed gas and raising the adsorption pressure favor the alternating transformation process of adsorbed and free gas molecules, enhancing the desorption process and leading to a higher diffusion coefficient.

https://doi.org/10.1021/acsomega.3c10156
ACS Omega 2024, 9, 16176−16186

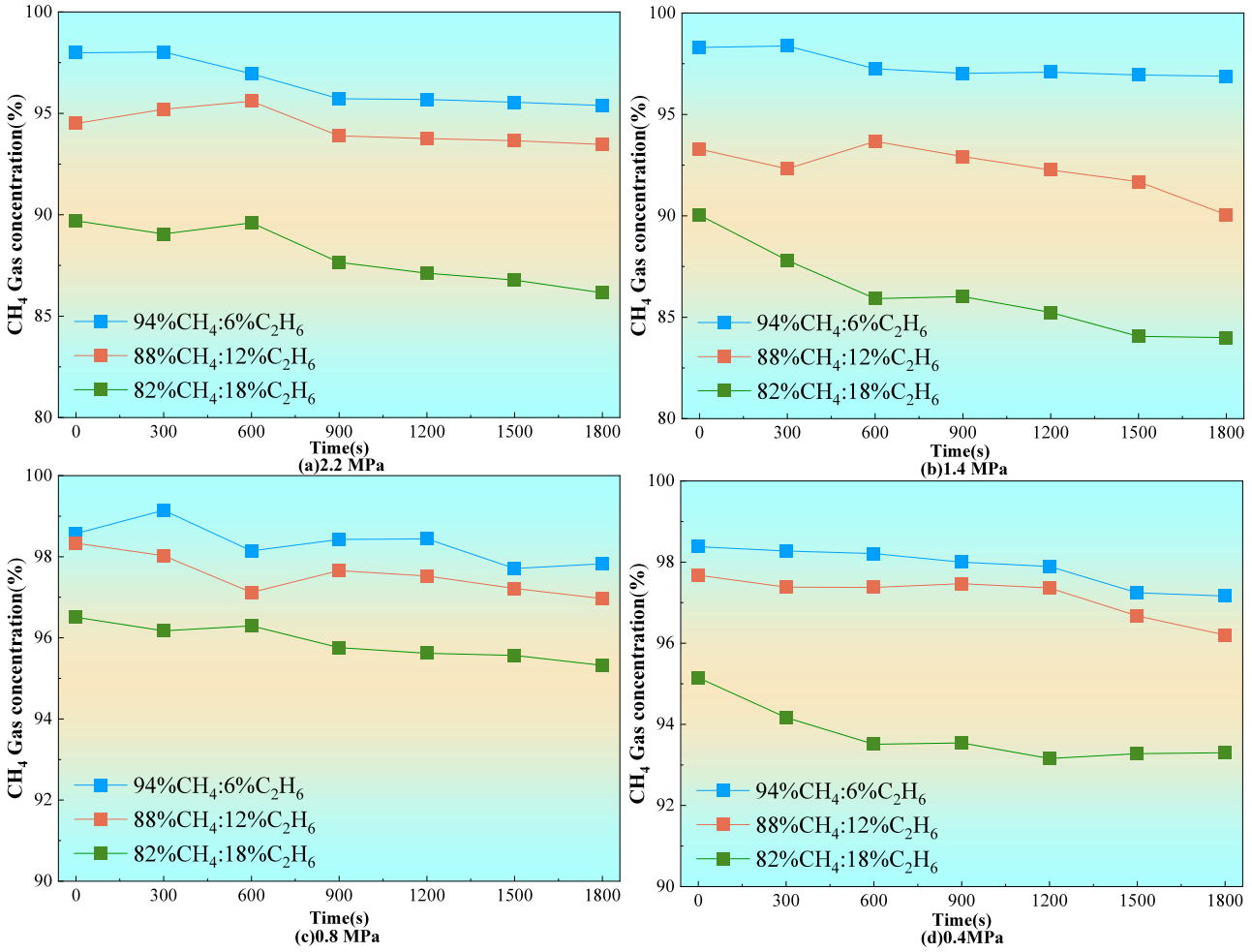

Figure 9. Temporal changes in CH_4 concentration during the desorption experiment of CH_4−C_2H_6 mixed gas under the same adsorption-equilibrium pressure.

3.3. Concentration Changes in the CH_4−C_2H_6 Mixed Gas. When coal adsorbs a heavy hydrocarbon gas, its inner surface is occupied by heavy hydrocarbon molecules, which displace some of the light hydrocarbon molecules, such as CH_4. The displaced constituents fill the pore spaces in the coal, affecting the concentration of the mixed gas. Therefore, the change rule of the CH_4−C_2H_6 mixed gas concentration was investigated during the isothermal desorption process.

The desorption during the first 1800s was divided into six parts, and six gas cylinders of the same volume were prepared. The gas cylinders were replaced at 300s intervals by controlling the valve. Finally, the gas was released into a gas collection bag. The mixed gas samples desorbed during the six time periods were collected for chromatographic analysis. Before the desorption experiment, the gas in the coal sample tank, which exists in the adsorption-equilibrium state, was sampled by a gas cylinder. The parameters were marked as time 0 by chromatographic analysis and then compared with the six stages after the desorption parameters.

Under the same adsorption-equilibrium pressure, the CH_4 concentration in the mixed gas slightly decreased during the desorption process. After the beginning of desorption, the CH_4 concentration exceeded the design concentration before adsorption. During most desorption periods, the concentration of CH_4 was smaller than that in the adsorption-equilibrium state. Furthermore, at different adsorption-equilibrium pressures, the concentration of CH_4 in the three mixed gases showed a similar trend and overall increased with the decrease of adsorption-equilibrium pressure.

Under the same adsorption-equilibrium pressure, the C_2H_6 concentration trended overall upward over time (Figure 10), but it was always lower than the design concentration before adsorption. During the desorption process, the concentration of C_2H_6 is often greater than that in the adsorption-equilibrium state and increases with the increase of the C_2H_6 ratio in the three gas. In addition, the concentration of C_2H_6 decreases with the decrease of the adsorption-equilibrium pressure at the same time.

Combining Figures 9 and 10, one observes that, before and after desorption, the CH_4 concentration always exceeded the design concentration but the C_2H_6 concentration was always smaller than the design concentration, indicating that CH_4 desorption is prioritized over C_2H_6 desorption. Change rules of the mixed gas concentration reflect the distribution characteristics of light hydrocarbon components on the outer surface and heavy hydrocarbon components on the inner surface of coal (Figure 11).

According to the Polanyi adsorption potential theory, the inner surface distribution constitutes the surface-adsorption phase of heavy hydrocarbon-rich coal. Therefore, the external free gas phase, surface-adsorption phase, and internal solid phase

https://doi.org/10.1021/acsomega.3c10156
ACS Omega 2024, 9, 16176−16186

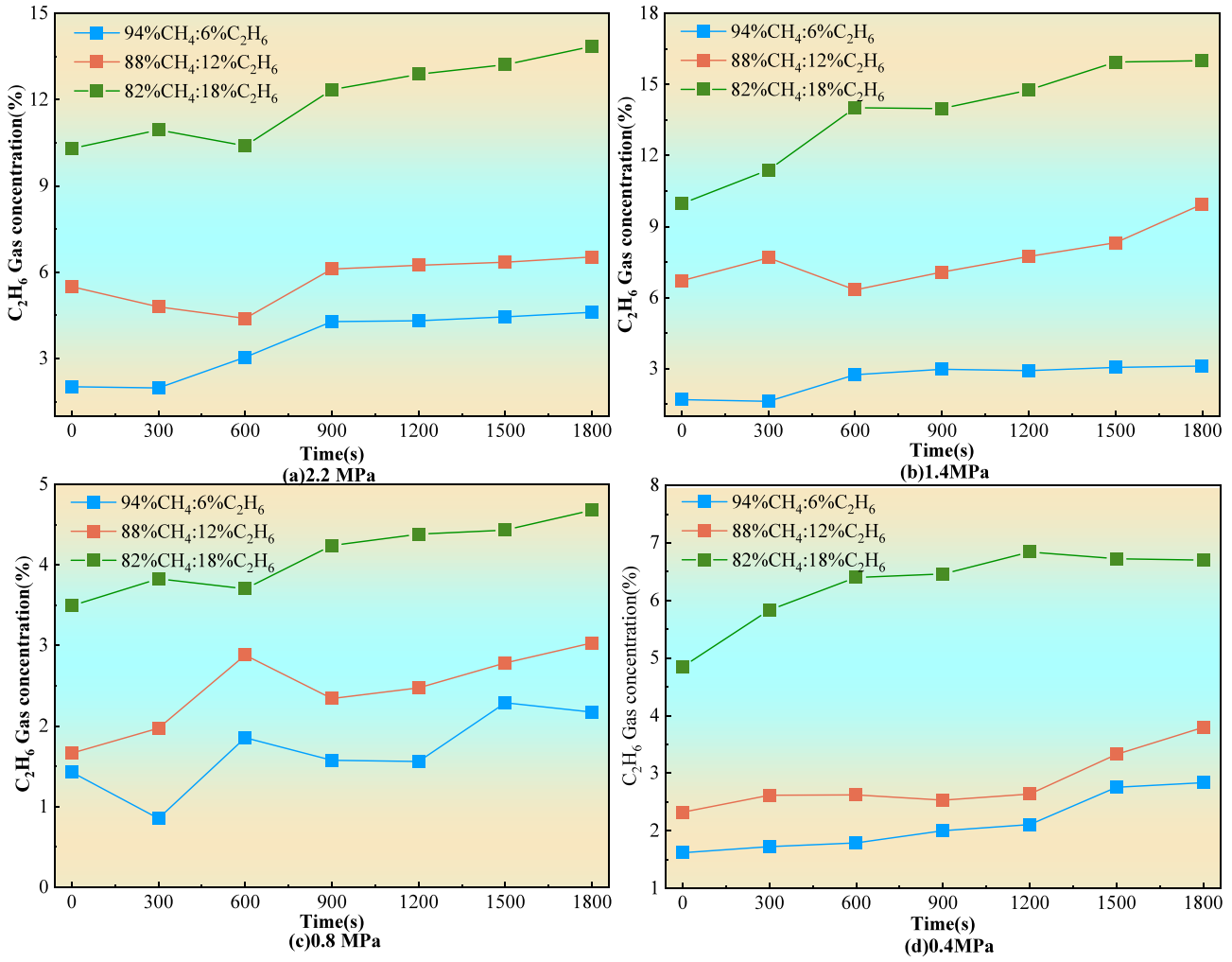

Figure 10. Temporal changes in C_2H_6 concentration during the desorption experiment of CH_4−C_2H_6 mixed gas under the same adsorption-equilibrium pressure.

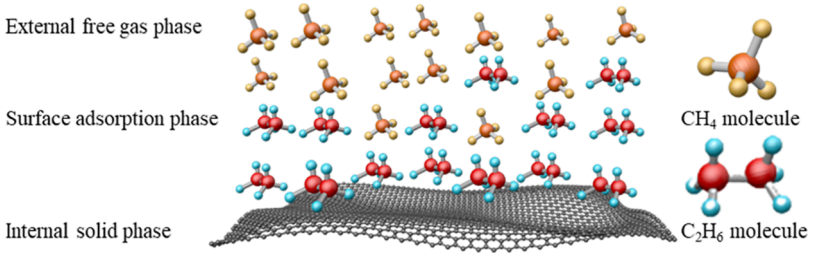

Figure 11. Three-phase adsorption structure model of heavy hydrocarbon-rich coal.

together constitute the three-phase adsorption structure of heavy hydrocarbon-rich coal.

4. CONCLUSIONS

1. The desorption volumes and rates of single-component CH_4 gas and C_2H_6 gas gradually increased with adsorption-equilibrium pressure. However, the desorption process decayed quickly during the first 1200s and more slowly thereafter. Under the same adsorption-equilibrium pressure, CH_4 was desorbed in higher quantity at higher speed than C_2H_6. As the adsorption-equilibrium pressure decreased, the difference between them decreased with the decrease of the adsorption-equilibrium pressure, with a tendency to approach each other.

2. Increasing the adsorption-equilibrium pressure increased the desorption quantity, desorption ratio, and diffusion coefficient of the CH_4−C_2H_6 mixed gas. Under the same adsorption-equilibrium pressure, the desorbed quantity and speed increased with increasing CH_4 concentration and decreased with increasing C_2H_6 concentration. The desorbed quantity of mixed gas exceeded those of the single-component gas. The desorption process largely depended on the concentration of heavy hydrocarbon gas. Increasing the C_2H_6 concentration gradually reduced the

https://doi.org/10.1021/acsomega.3c10156
ACS Omega 2024, 9, 16176−16186

diffusion coefficient of the CH_4−C_2H_6 mixed gas in the coal samples.

3. The desorption quantity of CH_4−C_2H_6 mixed gas increases rapidly with time and then tends to a stable value. The adsorption-equilibrium pressure significantly affects the desorption quantity of the mixed gas during the desorption process of the same concentration of CH_4−C_2H_6 mixed gas, which establishes a model of the desorption quantity of the mixed gas with different concentrations.
4. Decreasing the adsorption-equilibrium pressure increased the CH_4 concentration and decreased the C_2H_6 concentration. Under the same adsorption-equilibrium pressure, the CH_4 concentration slightly decreased while the C_2H_6 concentration increased overall. Comparing the results before and after desorption, the CH_4 concentration always exceeded the design concentration, indicating that CH_4 desorption is prioritized over C_2H_6 desorption. This behavior reflects the distribution characteristics of light hydrocarbon components on the outer coal surface and heavy hydrocarbon components on the inner coal surface.

■ ASSOCIATED CONTENT

Data Availability Statement

The data used to support the findings of this study are included within the article.

■ AUTHOR INFORMATION

Corresponding Authors

Yuehui Liang − *School of Safety Science and Engineering, Anhui University of Science and Technology, Huainan, Anhui 232001, China;* orcid.org/0009-0009-4808-4358; Email: yuehui@aust.edu.cn

Jiwei Yue − *School of Safety Science and Engineering, Anhui University of Science and Technology, Huainan, Anhui 232001, China; Technology Research and Development Platform for Disaster Prevention and Control Technology of Deep Coal Mining, Anhui University of Science and Technology, Huainan 232001, China; State Key Laboratory Cultivation Base for Gas Geology and Gas Control, Henan Polytechnic University, Jiaozuo 454000, China;* Email: yjwhpu@163.com

Authors

Biming Shi − *School of Safety Science and Engineering, Anhui University of Science and Technology, Huainan, Anhui 232001, China*

Chengcheng Zhang − *School of Safety Science and Engineering, Anhui University of Science and Technology, Huainan, Anhui 232001, China*

Xiaojing Shen − *School of Safety Science and Engineering, Anhui University of Science and Technology, Huainan, Anhui 232001, China*

Tao Hu − *School of Safety Science and Engineering, Anhui University of Science and Technology, Huainan, Anhui 232001, China;* orcid.org/0009-0000-6456-0902

Qijun Han − *School of Safety Science and Engineering, Anhui University of Science and Technology, Huainan, Anhui 232001, China;* orcid.org/0009-0001-5466-1483

Complete contact information is available at: https://pubs.acs.org/10.1021/acsomega.3c10156

Notes

The authors declare no competing financial interest.

■ ACKNOWLEDGMENTS

The authors are grateful for financial support from Anhui Provincial Natural Science Foundation (2308085QE152), National Natural Science Foundation of China (52304200 and U23A20601), Scientific and Technological Research Platform for Disaster Prevention and Control of Deep Coal Mining (Anhui University of Science and Technology) (NO. DPDCM2203), and the State Key Laboratory Cultivation Base for Gas Geology and Gas Control (Henan Polytechnic University) (NO. WS2022B03). The authors also appreciate the editor and the anonymous reviewers for their careful reviews of this paper.

■ REFERENCES

(1) Zhang, M.; Cao, X.; Zhang, L.; Zhou, A.; Li, B. Experimental study on the contribution of desorbed gas to the propagation and disaster-causing of coal-gas outbursts. *Fuel* **2023**, *349*, No. 128656.

(2) Liao, X. X.; Wang, B.; Wang, L.; Zhu, J. T.; Chu, P.; Zhu, Z. B.; Zheng, S. W. Experimental study on the wettability of coal with different metamorphism treated by surfactants for coal dust control. *ACS Omega* **2021**, *6* (34), 21925−21938.

(3) Meng, H.; Yang, Y. Z.; Guo, H. J.; Hou, W.; Li, X. W.; Chen, L.; Rong, T. L.; Yang, D. M.; Wang, C. L.; Shen, P. F. Experimental study on the determinant factors and energy criterion of coal and gas outbursts. *ACS Omega* **2023**, *8* (40), 37248−37263.

(4) Wang, L.; Cheng, L. B.; Cheng, Y. P.; Yin, G. Z.; Cai, C. C.; Xu, C.; Jin, K. Thermal effects of magmatic sills on coal seam metamorphism and gas occurrence. *Bull. Volcanol* **2014**, *76* (4), 1−16.

(5) Dutka, B. Effect of depth on the sorption capacity of coals affected by outburst hazard. *Fuel* **2021**, *306* (1), No. 121611.

(6) Yang, Y.; Zhang, X.; Zhou, X. F.; Wang, A. L.; Li, J. T. Real gas effect and bulk diffusion characteristics of shale mixed gas transport in microscale fractures. *ACS Omega* **2023**, *8* (19), 17077−17085.

(7) Li, Y. K.; Sun, S. Z.; Feng, D. D.; Zhang, W. D.; Zhao, Y. J.; Qin, Y. K. Syngas tempered pulverized coal reburning: Effect of different reaction gas components. *Energy* **2023**, *271*, No. 127080.

(8) Yue, J. W.; Wang, Z. F.; Dong, J. X.; Wang, C. G.; Shen, X. J. Law of water migration during spontaneous imbibition in loaded coal and its influence mechanism. *J. China Coal Soc.* **2022**, *47* (11), 4069−4082.

(9) Hou, X. W.; Liu, S. M.; Zhu, Y. M.; Yang, Y. Evaluation of gas contents for a multi-seam deep coalbed methane reservoir and their geological controls: In situ direct method versus indirect method. *Fuel* **2020**, *265*, No. 116917.

(10) Dai, X.; Wei, C.; Wang, M.; Shi, X.; Wang, X.; Vandeginste, V. Experimental investigation of storage space and adsorption capacity variation of shale under different reaction times in supercritical CO_2. *Nat. Resource Res.* **2023**, *32* (5), 2337−2353.

(11) Pei, L. X.; Gang, W. Z.; Zhu, C. Z.; Liu, Y. Z.; He, W. J.; Dong, Y. X.; Xiang, B. L. Carbon isotope and origin of the hydrocarbon gases in the Junggar Basin, China. *J. Nat. Gas. Geo. Sci.* **2018**, *3* (5), 253−261.

(12) Lan, F. J.; Qin, Y.; Wang, A.; Li, M.; Wang, G. The origin of high and variable concentrations of heavy hydrocarbon gases in coal from the Enhong syncline of Yunnan, China. *J. Nat. Gas Sci. Eng.* **2020**, *76*, No. 103217.

(13) Gentzis, T.; Goodarzi, F.; Cheung, F. K.; Laggoun-Défarge, F. Coalbed methane producibility from the mannville coals in Alberta, Canada: A comparison of two areas. *Int. J. Coal Geol* **2008**, *74*, 237−249.

(14) Formolo, M.; Martini, A.; Petsch, S. Biodegradation of sedimentary organic matter associated with coalbed methane in the Powder River and San Juan Basins, U.S.A. *Int. J. Coal Geol* **2008**, *76* (1−2), 86−97.

(15) Wang, H. J.; Liu, S. D.; Ma, L.; Shu, J. S.; Wang, X. Y.; Zhu, Y. Y. Controlling factors of abnormal heavy hydrocarbon content in

https://doi.org/10.1021/acsomega.3c10156
ACS Omega 2024, 9, 16176−16186

Huoshaopu mine field of Pansyncline. *J. China Coal Soc.* **2022**, *47* (9), 3421−3441.
(16) Zhang, B. X.; Fu, X. H.; Yu, K.; Tian, F. H.; Deng, Z. Geochemical composition and microstructure of coal measure shale in the upper permian, western Guizhou, China: implications for methane generation and storage. *Energy Fuels* **2022**, *36* (17), 10143−10154.
(17) Wang, K.; Ren, H. Y.; Wang, Z. F.; Ma, S. J.; Wei, J. J.; Ke, W.; Guo, Y. Y. Kinetic characteristics of CH_4 adsorption on coals under variable temperature−pressure coupling interaction. *Nat. Resour. Res.* **2021**, *30* (6), 4597−4620.
(18) Ji, B. N.; Pan, H. Y.; Pang, M. K.; Pan, M. Y.; Zhang, H.; Zhang, T. J. Molecular simulation of CH_4 adsorption characteristics in bituminous coal after different functional group fractures. *Energy* **2023**, *282*, No. 128967.
(19) Wang, K.; Pan, J. N.; Xu, R. T.; Hou, Q. L.; Wang, X. L.; Li, J. X. Macromolecular rearrangement caused by CO_2 adsorption in coal. *Fuel* **2023**, *349*, No. 128630.
(20) Zhang, S. S.; Liu, H.; Jin, Z. H.; Wu, C. F. Multifractal analysis of pore structure in middle- and high-rank coal by mercury intrusion porosimetry and low-pressure N_2 adsorption. *Nat. Resour. Res.* **2021**, *30* (6), 4565−4584.
(21) Yu, B. C.; Zhang, D. M.; Xu, B.; Xiao, W. J.; Wang, C. Y.; Du, W. H. Experimental study of desorption and seepage characteristics of single gas and CO_2-CH_4 gas mixture in coal. *Nat. Resour. Res.* **2022**, *31* (5), 2715−2730.
(22) Li, L.; Long, H.; Li, S. G.; Lin, H. F.; Qin, L.; Bai, Y.; Xiao, T. Permeability characteristics of CH_4, CO_2, and N_2 during the whole process of adsorption in coal with accumulated pressure under triaxial stresses. *J. Pet. Sci. Eng.* **2022**, *213*, No. 110380.
(23) Xu, C.; Wang, W. J.; Wang, K.; Zhou, A. T.; Guo, L.; Yang, T. Filling−adsorption mechanism and diffusive transport characteristics of N_2/CO_2 in coal: Experiment and molecular simulation. *Energy* **2023**, *282*, No. 128428.
(24) Long, H.; Lin, H. F.; Yan, M.; Bai, Y.; Tong, X.; Kong, X. G.; Li, S. G. Adsorption and diffusion characteristics of CH_4, CO_2, and N_2 in micropores and mesopores of bituminous coal: Molecular dynamics. *Fuel* **2021**, *292*, No. 120268.
(25) Xiao, T.; Li, S. G.; Long, H.; Kong, X. G.; Bai, Y.; Qin, A. L. Experimental research on adsorption characteristics of N_2, CH_4, and CO_2 in coal under different temperatures and gas pressures. *Energy Sci. Eng.* **2023**, *11* (2), 637−653.
(26) Li, Y.; Pan, J.; Cheng, N.; Wang, Z.; Zhang, L.; Liu, W. Relationship between micropore structure of different coal ranks and methane diffusion. *Nat. Resource Res.* **2022**, *31* (5), 2901−2917.
(27) Liu, Q. Q.; Wang, J.; Zhao, W.; Huang, W. Y.; Ling, H.; Wang, L.; Cheng, Y. P. A novel bidisperse diffusion model for coal particles considering micropores as the major sites of CH_4 adsorption. *Fuel* **2023**, *333*, No. 126505.
(28) Guatame, C.; Rincón, M.; Bermúdez, M. A. Relationship between coal composition, coal facies, and desorbed methane gas content: Thermal histories and exhumation processes in the middle Magdalena valley basin, Colombia. *J. South Am. Earth Sci.* **2023**, *128*, No. 104369.
(29) Sun, Y. X.; Wang, Z. F.; Yue, J. W.; Liang, Y. H. Study on gas desorption law and gas loss estimation in a positive pressure reverse circulation sampling process. *Fuel* **2023**, *352*, No. 129141.
(30) Yue, J. W.; Ma, Y. K.; Wang, Z. F.; Zhang, X.; Wang, L.; Shen, X. J. Characteristics of water migration during spontaneous imbibition in anisotropic coal. *Energy* **2023**, *263*, No. 126054.
(31) Morlanés, N.; Kavitake, S. G.; Rosenfeld, D. C.; Basset, J. M. Alkane cross-metathesis reaction between light and heavy linear alkanes, on a silica supported well-defined single-site catalyst. *ACS Catal.* **2019**, *9* (2), 1274−1282.
(32) Scafutto, R. D. M.; de Souza Filho, C. R. Detection of heavy hydrocarbon plumes (ethane, propane and butane) using airborne longwave (7.6−13.5μm) infrared hyperspectral data. *Fuel* **2019**, *242*, 863−870.
(33) Cesar, J.; Mayer, B.; Deblonde, C.; Mort, A.; H. Ardakani, O. Alternative indicators to assess the distribution characteristics of methane, ethane, and propane derived from petroleum in the Montney formation, Western Canada. *Fuel* **2021**, *294* (40), No. 120524.
(34) Wei, Q.; Zheng, K.; Hu, B. L.; Li, X. Q.; Feng, S. B.; Jiang, W.; Zhu, W. W.; Feng, W. Q. Methane adsorption capacity of deep-buried coals based on pore structure in the Panji deep area of Huainan coalfield, China. *Energy Fuels* **2021**, *35* (6), 4775−4790.
(35) Wei, Q.; Li, X. Q.; Hu, B. L.; Zhang, X. Q.; Zhang, J. Z.; He, Y. K.; Zhang, Y. C.; Zhu, W. W. Reservoir characteristics and coalbed methane resource evaluation of deep-buried coals: a case study of the No.13−1 coal seam from the Panji deep area in Huainan coalfield, southern north China. *J. Pet. Sci. Eng.* **2019**, *179*, 867−884.
(36) Cheng, X. J.; Wen, H.; Fan, S. X.; Chen, J.; Zhai, X. W.; Yu, Z. J.; Tong, X. Z.; Lei, C. X.; Xu, Y. H.; Cheng, B. K.; Li, R. K. Liquid CO_2 high-pressure fracturing of coal seam and gas extraction engineering tests using crossing holes: A case study of Panji coal mine No.3, Huainan, China. *Int. J. Energy Res.* **2021**, *45* (3), 4565−4580.
(37) Liu, H. H.; Lan, T. H.; Hu, B. L.; Xue, J. H.; Xu, H. J.; Zhang, W. Y.; Ren, B.; Huang, Y. H. Geochemical characteristics and its origins of CBM in deep-seated coal seam around Panji mining area of Huainan. *J. China Coal Soc.* **2018**, *43* (2), 498−506.
(38) Wang, L.; Wang, H.; Zhu, J. T.; Huang, W. Y.; Zhao, Y. C. Experimental study on particle size distribution of impact crushed coal containing gas. *Fuel* **2022**, *325*, No. 124745.
(39) Yue, J. W.; Wang, Z. F.; Shi, B. M.; Dong, J. X.; Shen, X. J. Interaction mechanism of water movement and gas desorption during spontaneous imbibition in gas-bearing coal. *Fuel* **2022**, *318*, No. 123669.
(40) Keshavarz, A.; Sakurovs, R.; Grigore, M.; Sayyafzadeh, M. Effect of maceral composition and coal rank on gas diffusion in Australian coals. *Int. J. Coal Geol.* **2017**, *173*, 65−75.

https://doi.org/10.1021/acsomega.3c10156
ACS Omega 2024, 9, 16176−16186